Commun Nonlinear Sci Numer Simulat 44 (2017) 74–88

Contents lists available at ScienceDirect

Commun Nonlinear Sci Numer Simulat

journal homepage: www.elsevier.com/locate/cnsns

Research paper

Dual effects of buoyancy and enstrophy transfer on scaling behavior of a shell model proposed for homogeneous turbulent convection

Yu Xing, Peiqing Liu, Hao Guo*

[a] Institute of Fluid Mechanics, Beihang University, Beijing 100191, People's Republic of China
[b] Key Laboratory of Fluid Mechanics (Beihang University), Ministry of Education, Beijing 100191, People's Republic of China

ARTICLE INFO

Article history:
Received 14 December 2015
Revised 6 May 2016
Accepted 22 July 2016
Available online 29 July 2016

Keywords:
Turbulent convection
SabraT model
Bolgiano-Obuchov scaling
Buoyancy

ABSTRACT

In this paper, we explain why the Bolgiano-Obukhov (BO) scaling behavior is unavailable by the SabraT model proposed for turbulent thermal convection in the range of $1 < \delta < 2$, which is extended from the Sabra model by coupling temperature with velocity in the equations of motion as an external forcing, i.e., buoyancy. Numerical studies show that SabraT model is mainly governed by the enstrophy budget equation, at which the buoyancy is not always relevant to the statistical properties and the effect of buoyancy is dependent on the parameter γ that measures the ratio of enstrophy to energy. When buoyancy is important, BO scaling is expected using theoretical arguments, such as dimensional analysis. Instead of BO scaling, a new γ-dependent scaling behavior is setup in the buoyancy relevant regime, which is found to equivalently deviate from the enstrophy cascade scaling and BO scaling. This deviation is mainly discussed by two dimensionless parameters, which respectively measure the deviation of the energy/enstrophy transfer flux rate and the injected energy/enstrophy due to buoyancy from dimensional analysis. The introduced buoyancy plays as a relative small perturbed forcing on the Sabra model without changing much its intrinsical statistical properties, i.e., dimensional analysis is not always validated in both Sabra and SabraT models.

1. Introduction

Appearing in many natural phenomena and technological applications, turbulent thermal convection is a problem of great research interest [1,2], which is driven by buoyancy forces generated by temperature differences. One interesting issue is to understand the scaling behavior of the velocity and temperature fluctuations in the inertial range of scales in which buoyancy is relevant or irrelevant [3]. It has been proposed [4] that when buoyancy is dominant and temperature acts as an active scalar, the scaling behavior of velocity and temperature are governed by a direct entropy cascade of constant entropy flux with inverse energy transfer flux and would be described by the Bolgiano and Obukhov (BO) scaling [5] plus corrections [6,7] in the range containing scales between the Bolgiano length scale L_B [8], and the large scale of the system L_0, that determined by geometry. Recently, Zhou numerically verified these phenomenon by investigation of the two-dimensional (2D) Rayleigh-Taylor turbulence, where the mean kinetic energy is dynamically transferred to large scales by an inverse

* Corresponding author.
E-mail address: guohao@buaa.edu.cn (H. Guo).

http://dx.doi.org/10.1016/j.cnsns.2016.07.019
1007-5704/

cascade, while both the mean thermal energy or entropy and the mean enstrophy move towards small scales by forward cascades [9]. When buoyancy is irrelevant and temperature acts as a passive scalar in the range of $L < L_B$, the scaling behaviors are governed by entropy and energy cascades and would be described by Kolmogorov 1941 (K41) scaling [10] plus intermittency corrections, which has been verified in the time scale by Ching [11] and Zhou [12].

In order to understand the buoyancy-driven turbulent phenomenology, many different techniques and approximations have been developed, such as shell models. Shell models focussing on the energy cascade process have been studied intensively and proved to be useful for understanding the scaling behavior of velocity fluctuations in inertia-driven turbulence (see, for example, [13] for a review). Two classes of shell models have been proposed for studying homogeneous and isotropic turbulence. The first class consists of the shell model proposed by Desnyansky and Novikov [14], in which different scaling behaviors are observed due to different attractive fixed-point solutions [15]. The other class consists of the Gledzer-Ohkitani-Yamada (GOY) model [16] and its improved model, i.e., the Sabra model [17], which is proposed to eliminate some undesirable periodic oscillation in the GOY model. In the GOY or Sabra model, the scaling behavior is dependent on model parameter δ, i.e., K41 scaling is set up in the range of $0 < \delta < 1$ for 3D turbulent flow and energy/enstrophy equipartition and cascades scalings are set up in the range of $1 < \delta < 2$ for 2D turbulent flow [18,19]. The inviscid invariants, like the energy and enstrophy, are important quantities determining the dynamics of the Sabra model.

Two classes of shell models are correspondingly constructed for turbulent thermal convection. For the first class, both BO scaling and K41 scaling behaviors have been reported in the shell model first constructed by Brandenburg [20] and also in the modified model by Suzuki and Toh [21] for some parameter range. Fruitful following theoretical and numerical results have been reported by us from the Brandenburg model, such as scalings and heat flux transfer issues for turbulent homogeneous convection [7,22,23]. For the second class, K41 scaling has been reported by Jiang and Liu [24] using a shell model extended from the GOY model. In the range of $0 < \delta < 1$, K41 scaling plus intermittency corrections is also set up by the SabraT model [25], extended from the Sabra model. Thus, buoyancy is found to be not always significant and relevant to the statistical properties in these shell models even though there is an explicit coupling term with temperature in the equation of motion for velocity [22]. Recently, the Sabra model is also modified to study other turbulent issues, apart from turbulent homogeneous convection. Based on the Sabra model, a 2D-3D shell model is constructed for investigating the phenomenology of turbulent cascades in fluid layers with large aspect ratio, namely Rayleigh-Taylor convection [26]. Besides the convective turbulence, shell models can be used to study another buoyancy-driven turbulence, such as stably stratified turbulence [27–32]. A unified shell model for stably stratified and convective turbulence is also constructed from the Sabra model to yield BO scaling for stably stratified flows and K41 scaling for convective turbulence [33]. Moreover, K41 scaling has been reported in most of these models while BO scaling is only reported in the first class of shell model, i.e., Brandenburg model with suitable parameters. In particular, there is the natural question of why BO scaling is unavailable in the second class of shell model proposed for turbulent homogeneous convection, i.e., the SabraT model.

In this paper, we focus on studying the SabraT model in the range of $1 < \delta < 2$. In Section 2, we describe the SabraT model with the Sabra model. In Section 3, we study the observed scaling behavior of velocity in the SabraT model. In this section, we show that four regimes exist with different buoyant effects. A modified enstrophy cascade scaling behavior, instead of BO scaling and enstrophy cascade scaling, is set up in regime (III). In Section 4, buoyancy effects of the SabraT model is discussed. Finally, we end this paper with a discussion and conclusion in Section 5.

2. The SabraT model

In the Boussinesq approximation, the dynamical equations that describe the homogeneous turbulent convection that driven by a constant temperature gradient along the vertical direction are

$$\frac{\partial \vec{V}}{\partial t} + \vec{V}\cdot\nabla\vec{V} = -\nabla p + \nu\nabla^2\vec{V} + \alpha g\theta\hat{z}, \tag{1}$$

$$\frac{\partial \theta}{\partial t} + \vec{V}\cdot\nabla\theta = \kappa\nabla^2\theta + \beta V_z \tag{2}$$

with $\nabla\cdot\vec{V} = 0$. Here, $\vec{V}$ is the velocity field, $\theta = (T - T_0 - \beta z)$ is the deviation of temperature from a linear gradient $-\beta$, T_0 is the mean temperature of the fluid, p is the pressure divided by the density, and $\hat{z}$ is a unit vector in the vertical direction. Furthermore, g is the acceleration due to gravity and α, ν, κ are, respectively, the volume expansion coefficient, the kinematic viscosity and thermal diffusivity of the fluid.

The SabraT model has been proposed for studying the homogeneous turbulent convection driven by a temperature gradient. The basic idea of shell model is to construct a set of ordinary differential equations of fluid mechanics in wave-vector representation, “shells”, taking into account only a few variables per shell, such as u_n and θ_n. These variables can be roughly thought of as the Fourier transforms of the velocity and temperature fields with wavevector $\vec{k}$, whose magnitude satisfies $k_n \le |\vec{k}| \le k_{n+1}$. Here, $k_n = 2^n k_0$ is the wavenumber of the nth shell, with $0 \le n < N$, and $k_0 = 1$ is the wavenumber corresponding to the largest scale in the system.

In the SabraT model, u_n and θ_n are complex and satisfy the following equations of motion:

$$\frac{du_n}{dt} = ik_{n+1}\left(u^*_{n+1}u_{n+2} - \frac{\delta}{2}u^*_{n-1}u_{n+1} + \frac{1-\delta}{4}u_{n-1}u_{n-2}\right) - \nu k_n^2 u_n - D_n u_n + f_n \tag{3}$$

$$\frac{d\theta_n}{dt} = ik_n(\theta_{n-1}u^*_n + 2\theta_{n+1}u_{n+1}) - \kappa k_n^2\theta_n + \beta u_n \tag{4}$$

where f_n and D_n are the external driving and drag force, respectively. The drag forcing is important only at large scales and usually chosen as $D_n = \mu k_n^{-2}$, where μ is the friction coefficient. For the Sabra model, the driving force is temperature independent and active on a few shells near the shell $n = n_f$, e.g., $f_n = f_0\delta_{n,n_f}$; whereas, for the SabraT model, the driving force (buoyancy) is active on each shell with the form of $f_n = \alpha g\theta_n$.

In the limit of $\nu \to 0$ and $\kappa \to 0$, shell model is always constructed to satisfy conservation laws of kinetic energy and entropy (proportional to $|\theta_n|^2$) with flux-like form of nonlinear terms in the evolution equations of kinetic energy and entropy in the nth shell. For the Sabra model, it was reported that one more definite invariant, i.e., the "enstrophy" $H = k_n^\gamma E$, exists in the range of $1 < \delta < 2$, in addition to the conservation of energy E. Here, $\gamma = -\log_2(\delta - 1)$. For the SabraT model, one gets the following average budget equations of energy, enstrophy and entropy

$$\frac{1}{2}\frac{d}{dt}\langle S_2(k_n)\rangle = \langle F_u(k_n)\rangle - \langle F_u(k_{n+1})\rangle - \langle D_u(k_n)\rangle + \langle P_u(k_n)\rangle - \langle Q(k_n)\rangle \tag{5}$$

$$\frac{1}{2}\frac{d}{dt}\left\langle \tilde{S}_2(k_n)\right\rangle = \left\langle \tilde{F}_u(k_n)\right\rangle - \left\langle \tilde{F}_u(k_{n+1})\right\rangle - \left\langle \tilde{D}_u(k_n)\right\rangle + \left\langle \tilde{P}_u(k_n)\right\rangle - \left\langle \tilde{Q}(k_n)\right\rangle \tag{6}$$

$$\frac{1}{2}\frac{d}{dt}\langle R_2(k_n)\rangle = \langle F_\theta(k_n)\rangle - \langle F_\theta(k_{n+1})\rangle - \langle D_\theta(k_n)\rangle + \langle P_\theta(k_n)\rangle \tag{7}$$

where $\langle ...\rangle$ denotes a time average. Here, the containing, dissipation, injected and output energy at each shell are $S_2(k_n) = |u_n|^2$, $D_u(k_n) = \nu k_n^2 S_2(k_n)$, $P_u(k_n) = Re\{f_n u_n^*\}$ and $Q(k_n) = D_n S_2(k_n)$, respectively; the containing, dissipation, injected and output enstrophy at each shell are $\tilde{S}_2(k_n) = k_n^\gamma S_2(k_n)$, $\tilde{D}_u(k_n) = k_n^\gamma D_u(k_n)$, $\tilde{P}_u(k_n) = k_n^\gamma P_u(k_n)$, $\tilde{Q}(k_n) = k_n^\gamma Q(k_n)$, respectively; and the containing, dissipation and input entropy at each shell are $R_2(k_n) = |\theta_n|^2$, $D_\theta(k_n) = \kappa k_n^2 R_2(k_n)$, and $P_\theta(k_n) = \beta Re\{u_n\theta_n^*\}$, respectively; $F_u(k_n)$, $\tilde{F}_u(k_n)$ and $F_\theta(k_n)$ are respectively the rate of energy/enstrophy/entropy transfer or energy/enstrophy/entropy flux from $(n-1)$th to nth shell, which are given as

$$F_u(k_n) = \Delta_n - (\delta - 1)\Delta_{n-1} \tag{8}$$

$$\tilde{F}_u(k_n) = (\delta - 1)\tilde{\Delta}_n - \tilde{\Delta}_{n-1} \tag{9}$$

$$F_\theta(k_n) = Im\left\{k_n\theta^*_{n-1}\theta_n u_n\right\} \tag{10}$$

where $\Delta_n = k_n\hat{S}_3(k_n)$, $\tilde{\Delta}_n = k_n^\gamma\Delta_n = k_n^{1+\gamma}\hat{S}_3(k_n)$ and $\hat{S}_3(k_n) = \mathrm{Im}\left\{u^*_{n-1}u^*_n u_{n+1}\right\}$.

In the stationary state, summation of Eq. (5) and (6) from $n > 1$ to $N-1$ gives

$$\langle F_u(k_n)\rangle = \sum_n^{N-1}\langle D_u(k_m)\rangle - \sum_n^{N-1}\langle P_u(k_m)\rangle + \sum_n^{N-1}\langle Q(k_m)\rangle \tag{11}$$

$$\left\langle \tilde{F}_u(k_n)\right\rangle = \sum_n^{N-1}\left\langle \tilde{D}_u(k_m)\right\rangle - \sum_n^{N-1}\left\langle \tilde{P}_u(k_m)\right\rangle + \sum_n^{N-1}\left\langle \tilde{Q}(k_m)\right\rangle \tag{12}$$

Thus, one gets

$$\varepsilon_t = \varepsilon_u + \varepsilon_d \tag{13}$$

$$\tilde{\varepsilon}_t = \tilde{\varepsilon}_u + \tilde{\varepsilon}_d \tag{14}$$

where $\varepsilon_t = \sum_0^{N-1}\langle P_u(k_n)\rangle$ and $\tilde{\varepsilon}_t = \sum_0^{N-1}\left\langle \tilde{P}_u(k_n)\right\rangle$ are respectively the total energy/enstrophy dissipation rate that equals to the injected energy/enstrophy rate; $\varepsilon_u = \sum_0^{N-1}\langle D_u(k_n)\rangle$ and $\tilde{\varepsilon}_u = \sum_0^{N-1}\left\langle \tilde{D}_u(k_n)\right\rangle$ are respectively the local energy/enstrophy dissipation rate; $\varepsilon_d = \sum_0^{N-1}\langle Q(k_n)\rangle$ and $\tilde{\varepsilon}_d = \sum_0^{N-1}\left\langle \tilde{Q}(k_n)\right\rangle$ are respectively the average energy/enstrophy dissipation due to friction drag. Similarly, one gets the local entropy dissipation rate $\varepsilon_\theta = \sum_0^{N-1}\langle D_\theta(k_n)\rangle = \sum_0^{N-1}\langle P_\theta(k_n)\rangle$.

Two characteristic scales, namely the largest scale and the dissipation scale, are usually denote as k_0 and k_d in shell models, respectively. In the scaling range, $k_0 \ll k_n \ll k_d$, both local dissipation due to viscosity and friction drag are negligible in comparison with the nonlinear interactions among shells, i.e., $\sum_0^{n-1} \langle D_u(k_m)\rangle \approx \sum_0^{n-1} \left\langle \tilde{D}_u(k_m)\right\rangle \approx \sum_0^{n-1} \langle D_\theta(k_m)\rangle \approx 0$ and $\sum_n^{N-1} \langle Q(k_m)\rangle \approx \sum_n^{N-1} \left\langle \tilde{Q}(k_m)\right\rangle \approx 0$. Thus, from Eq. (8) to (10), one gets

$$\langle F_u(k_n)\rangle \approx \varepsilon_u - P_n \tag{15}$$

$$\left\langle \tilde{F}_u(k_n)\right\rangle \approx \tilde{\varepsilon}_u - \tilde{P}_n \tag{16}$$

$$\langle F_\theta(k_n)\rangle \approx \varepsilon_\theta - B_n \tag{17}$$

where the different terms excited by the external forcing are defined as $P_n = \sum_n^{N-1} \langle P_u(k_m)\rangle$ and $\tilde{P}_n = \sum_n^{N-1} \left\langle \tilde{P}_u(k_m)\right\rangle$ and $B_n = \sum_n^{N-1} \langle P_\theta(k_m)\rangle$. Clearly, when the transfer flux is scale independent, a cascade of the conserved invariant (energy/enstrophy/entropy) is setup in the scaling range, which suggests that the above forcing term is either scale independent with constant value or much smaller than the transfer flux that equals to the local dissipation rate. On the other hand, when the forcing term is scale dependent with large value, the transfer flux is scale dependent. Thus, the forcing term may play an important role in the scaling behavior of velocity and temperature, which is usually investigated by the velocity and temperature structure functions, defined by

$$\langle S_p(k_n)\rangle = \left\langle |u_n|^p\right\rangle \sim k_n^{-\zeta_p} \tag{18}$$

$$\langle R_p(k_n)\rangle = \left\langle |\theta_n|^p\right\rangle \sim k_n^{-\xi_p} \tag{19}$$

The K41 scaling would be characterized by $\zeta_p = \xi_p = p/3$ while the BO scaling by $\zeta_p = 3p/5$ and $\xi_p = p/5$.

For the Sabra model, the external driving force is active on the shell $k_n = k_f$, which is away from the largest scale k_0 and the dissipation scale k_d, i.e., $k_0 \ll k_f \ll k_d$. It is apparent that the external forcing terms P_n and $\tilde{P}_n$ are scale independent with different constant values across the forcing scale k_f, i.e., $P_n = \tilde{P}_n = 0$ for $k_n \gg k_f$, $P_n = \varepsilon_t$ and $\tilde{P}_n = \tilde{\varepsilon}_t$ for $k_n \ll k_f$. In the scaling range of $k_f \ll k_n \ll k_d$, one gets

$$\langle F_u(k_n)\rangle \approx \varepsilon_u \tag{20}$$

$$\left\langle \tilde{F}_u(k_n)\right\rangle \approx \tilde{\varepsilon}_u \tag{21}$$

which suggests that a direct cascade of energy/enstrophy is set up. In the range of $k_0 \ll k_n \ll k_f$, one gets

$$\langle F_u(k_n)\rangle \approx \varepsilon_u - \varepsilon_t = -\varepsilon_d \tag{22}$$

$$\left\langle \tilde{F}_u(k_n)\right\rangle \approx \tilde{\varepsilon}_u - \tilde{\varepsilon}_t = -\tilde{\varepsilon}_d \tag{23}$$

As the drag dissipation rate of energy/enstrophy is positive, the transfer flux of energy/enstrophy is negative, which suggests that an inverse cascade of energy/enstrophy is set up. Thus, for the Sabra model, a direct/inverse cascade of energy/enstrophy is possibly setup below/above the forcing scale with different scaling behaviors. It has been reported that a direct enstrophy cascade is observed in the range of $k_n > k_f$ for $1.25 < \delta < 2$ $(0 < \gamma < 2)$ [18] and an inverse energy cascade is observed in the range of $k_n < k_f$ for $1 + 2^{-2/3} < \delta < 2$ $(0 < \gamma < 2/3)$ [19].

Moreover, either energy/enstrophy cascades or diffusion in a statistical equilibrium has been observed and investigated in the Sabra model by the skewness [19]

$$R(k_n) = \frac{\left\langle \hat{S}_3(k_n)\right\rangle}{\langle S_2(k_n)\rangle^{3/2}} \sim k_n^\rho \tag{24}$$

which dimensionally measures the deviation of $\hat{S}_3$ from their standard deviation with Gaussian behavior. Here, a scaling exponent of ρ is supposed for dimensional analysis. As $\hat{S}_3$ relates to the rates of energy and enstrophy flux, one gets $\left\langle \hat{S}_3(k_n)\right\rangle \sim k_n^{\rho-\frac{3}{2}\zeta_2}$, which gives the scaling behavior of the energy and enstrophy flux rates

$$\langle F_u(k_n)\rangle \sim \langle \Delta(k_n)\rangle \sim \left\langle k_n \hat{S}_3(k_n)\right\rangle \sim k_n^{1+\rho-\frac{3}{2}\zeta_2} \tag{25}$$

and

$$\left\langle \tilde{F}_u(k_n)\right\rangle \sim \left\langle \tilde{\Delta}(k_n)\right\rangle \sim \left\langle k_n^{1+\gamma} \hat{S}_3(k_n)\right\rangle \sim k_n^{1+\gamma+\rho-\frac{3}{2}\zeta_2} \tag{26}$$

From dimensional analysis, $\rho = 0$ is expected with $R \sim k_n^0$. However, R is reported to be minimal at $k_n = k_c$ and increase to the order of unity at the dissipative boundaries $k_n = k_d$, i.e., $\rho < 0$ for $k_n < k_c$ and $\rho \geq 0$ for $k_n > k_c$. Both energy and enstrophy diffusion or equipartition scaling, i.e., $\zeta_2 = 0$ and $\zeta_2 = \gamma$, are observed below and above the critical shell k_c in the range of $1 < \delta < 1 + 2^{-2/3}$ ($0 < \gamma < 2/3$), where numerical small parameter of R is respectively expected with non-zero values of ρ, i.e., $\rho = -1$ and $\rho = -1 + 3\gamma/2$. When energy/enstrophy cascade is setup, constant small parameter of R is expected with $\rho = 0$, which gives the scaling exponents of $\zeta_2 = 2/3$ and $\zeta_2 = 2(1+\gamma)/3$, respectively. Obviously, dimensional prediction is not established for $\rho \neq 0$, and vice versa. Conclusively, the different scaling behaviors of the Sabra model are mainly due to the statistics of this ratio, R, which is always smaller than unity and has to approach saturation of the bound at the viscous dissipative boundary with the following constraint

$$\rho \geq 0 \tag{27}$$

As discussed laterly, this feature of R even plays an important role in the SabraT model, especially when $\rho \neq 0$.

Similarly, the buoyancy effect on the scaling behavior of velocity and temperature can be measured dimensionally by the ratio of the injected enstrophy due to buoyancy and the rate of enstrophy flux in the SabraT model

$$R_B(k_n) = \frac{\left\langle \tilde{P}_u \right\rangle}{\left\langle \tilde{F}_u \right\rangle} \sim k_n^{\rho_B} \tag{28}$$

with a supposed scaling exponent of ρ_B that determined by the scaling behavior of $\left\langle \tilde{P}_u \right\rangle$ and $\left\langle \tilde{F}_u \right\rangle$. As the rate of enstrophy flux is important in shell models, $\rho_B \leq 0$ is expected. When $\rho_B < 0$, one gets $R_B \ll 1$, which suggests that buoyancy is irrelevant in the scaling range. When $\rho_B = 0$, one gets $\left\langle \tilde{P}_u \right\rangle \sim \left\langle \tilde{F}_u \right\rangle$, which suggests that buoyancy is relevant in the scaling range. Thus, $\rho_B = 0$ is a critical value that determines the effect of buoyancy from dimensional analysis, i.e., buoyancy is irrelevant and relevant in the scaling range for $\rho_B < 0$ and $\rho_B = 0$, respectively.

From the definition of $\left\langle \tilde{P}_u \right\rangle$, the scaling exponent of ρ_B can be measured from the following cross correlation functions of velocity and temperature in the SabraT model

$$R_c(k_n) = \frac{\langle \mathrm{Re}\{u_n^* \theta_n\} \rangle}{\sqrt{\langle S_2(k_n) \rangle \langle R_2(k_n) \rangle}} = (\alpha g)^{-1} k_n^{-\gamma} \frac{\left\langle \tilde{P}_u(k_n) \right\rangle}{\sqrt{\langle S_2(k_n) \rangle \langle R_2(k_n) \rangle}} \sim k_n^{\rho_c} \tag{29}$$

with a scaling exponent ρ_c. Accordingly, one gets the scaling behavior of the injected enstrophy due to buoyancy

$$\left\langle \tilde{P}_u(k_n) \right\rangle \sim k_n^{\gamma + \rho_c - \frac{1}{2}\zeta_2 - \frac{1}{2}\xi_2} \tag{30}$$

and the scaling exponent in Eq. (28)

$$\rho_B = \rho_c - \rho + \zeta_2 - \frac{\xi_2}{2} - 1 \tag{31}$$

As the external forcing is adding on each shell, the forcing terms in Eq. (17) are scale dependent. However, numerical results show that the entropy cascade is always setup with $\langle F_\theta(k_n) \rangle \approx \langle \varepsilon_\theta \rangle \gg B_n$ for the SabraT model. From dimensional analysis, one gets

$$\langle F_\theta(k_n) \rangle \sim k_n u_n \theta_n^2 \sim k_n \langle S_2 \rangle^{1/2} \langle R_2 \rangle \sim k_n^{1 - \frac{1}{2}\zeta_2 - \xi_2} \approx \langle \varepsilon_\theta \rangle \sim k_n^0 \tag{32}$$

which gives the dependence of the two scaling exponents, i.e.,

$$\xi_2 = 1 - \frac{1}{2}\zeta_2 \tag{33}$$

Applying Eq. (33) to (31), one gets

$$\rho_B = \rho_c - \rho + \frac{5}{4}\zeta_2 - \frac{3}{2} \tag{34}$$

from the above dimensional analysis.

When buoyancy is irrelevant with the existence of energy and enstrophy cascades or diffusion in a statistical equilibrium, one gets the same scaling behavior of the SabraT model as the Sabra model. From the existence of energy and enstrophy equipartition scaling, one gets $\rho = -1$ and $\zeta_2 = 0$ for $k_n < k_c$, and $\rho = -1 + 3/2\gamma$ and $\zeta_2 = \gamma$ for $k_n > k_c$, respectively. From the existence of direct energy and enstrophy cascades, one gets $\langle F_u(k_n) \rangle \approx \varepsilon_\theta \gg P_n$ and $\left\langle \tilde{F}_u(k_n) \right\rangle \approx \tilde{\varepsilon}_\theta \gg \tilde{P}_n$, which suggests that buoyancy is only active in the regime near the largest scale k_0 and acts irrelevantly as a similar external forcing operated at shell k_0 in the Sabra model. Thus, one gets $\rho = 0$ and $\zeta_2 = 2(1+\gamma)/3$. As buoyancy is irrelevant, one gets $\rho_B < 0$ with $\rho_c < (4 - 5\gamma)/6$ from dimensional results of Eq. (31).

On the other hand, when the buoyancy term in Eq. (15) and (16) is scale dependent with large value, one gets $\rho_B = 0$ with relevant buoyancy, i.e.,

$$\left\langle \tilde{P}_u(k_n) \right\rangle \sim \left\langle \tilde{F}_u(k_n) \right\rangle \sim k_n^{1 + \gamma + \rho - \frac{3}{2}\zeta_2} \tag{35}$$

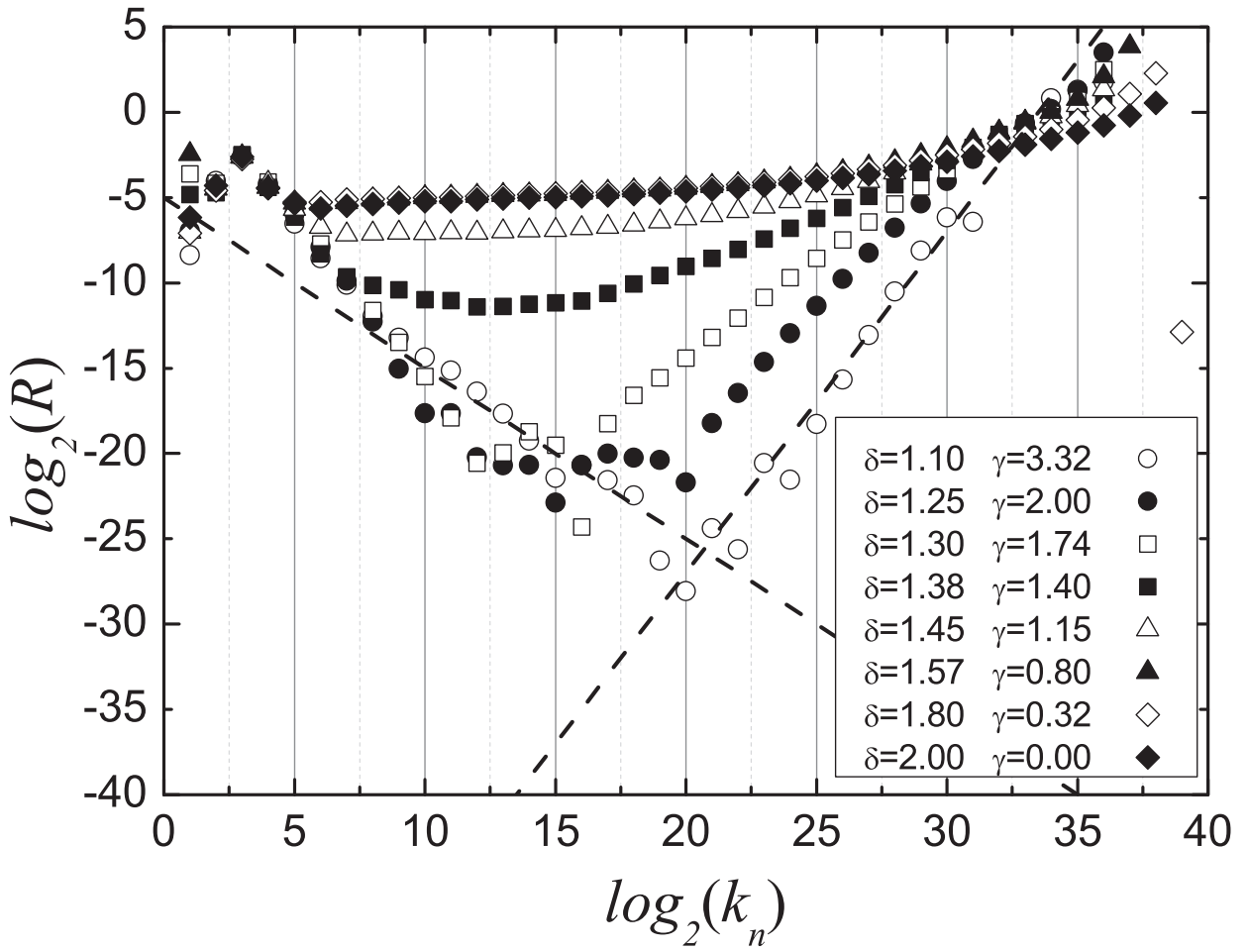

Fig. 1. A log-log plot of the skewness $R(k_n)$ as a function of k_n for different values of δ and γ. The dash lines show k_n^{-1} and $k_n^{-1+3\gamma/2}$ with $\gamma = 2$, respectively. Here, $\gamma = -\log_2(\delta - 1)$.

The scaling behavior of velocity may be influenced by buoyancy. From Eq. (31), one gets the second order scaling exponent of velocity

$$\zeta_2 = \frac{6}{5} + \frac{4}{5}(\rho - \rho_c) \tag{36}$$

which may deviate from the Bolgiano-Obukhov scaling exponent $\zeta_2 = 6/5$ when $\rho_c \neq \rho$. As discussed above, the existence of Bolgiano-Obukhov scaling is only observed when the following three conditions are satisfied: i) Eq. (33), which indicates dimensional analysis is available for the entropy cascade; ii) Eq. (35) with $\rho_B = 0$, which indicates buoyancy is relevant with large values that are of the same order as the enstrophy flux rate; iii) $\rho_c = \rho$, which indicates that R_c is of the same scale dependence as R. In the following section, these conditions are numerically detected with varying δ.

3. Scaling behavior of velocity in the SabraT model

We numerically integrate Eqs. (3) and (4) using the fourth-order Runge-Kutta method. The values of the parameters used in the simulations are $\alpha g = \beta = 1$, $\nu = \kappa = 10^{-16}$, $\mu = 1000$ and $k_0 = 1$. The corresponding Rayleigh number in present simulations is $Ra = \frac{\alpha g \beta}{k_0^4 \nu \kappa} = 10^{32}$ [33]. It was shown before that K41 scaling is observed in the range of $0 < \delta < 1$ with irrelevant buoyancy in the SabraT model. In this paper, we focus on $1 < \delta < 2$ with $\gamma > 0$.

As shown in Fig. 1, the skewness $R(k_n)$ measured in the SabraT model shows different dependence on k_n in different ranges of δ and γ. In the range of $1 + 2^{-0.8} < \delta < 2$ or $0 < \gamma < 0.8$, the skewness is parameter δ or γ independent and yields a number of the order of 0.03 that scales as k_n^{ρ} with $\rho = 0$, which suggests that a similar dependence of R on k_n is observed for the SabraT and Sabra model. Thus, the scaling behavior of the SabraT model is expected to be unchanged with irrelevant buoyancy in this range. When δ decreases from the critical value of $\delta = 1 + 2^{-0.8} \approx 1.57$ or γ increases from

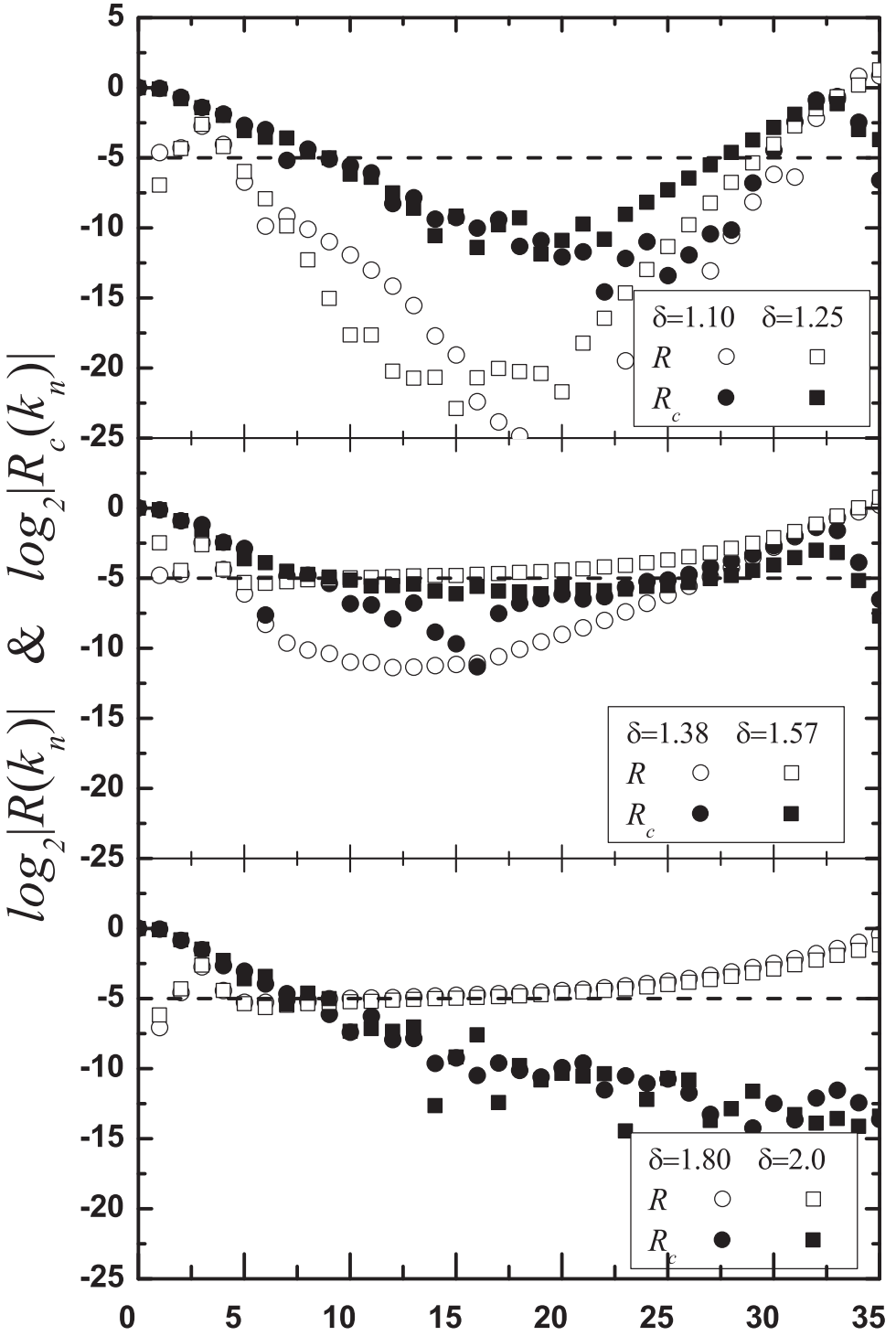

Fig. 2. A log-log plot of the skewness $R(k_n)$ (open symbols) and the cross correlation function $R_C(k_n)$ (closed symbols) as a function of k_n for different values of δ and γ. The line shows $k_n^{-2/3}$.

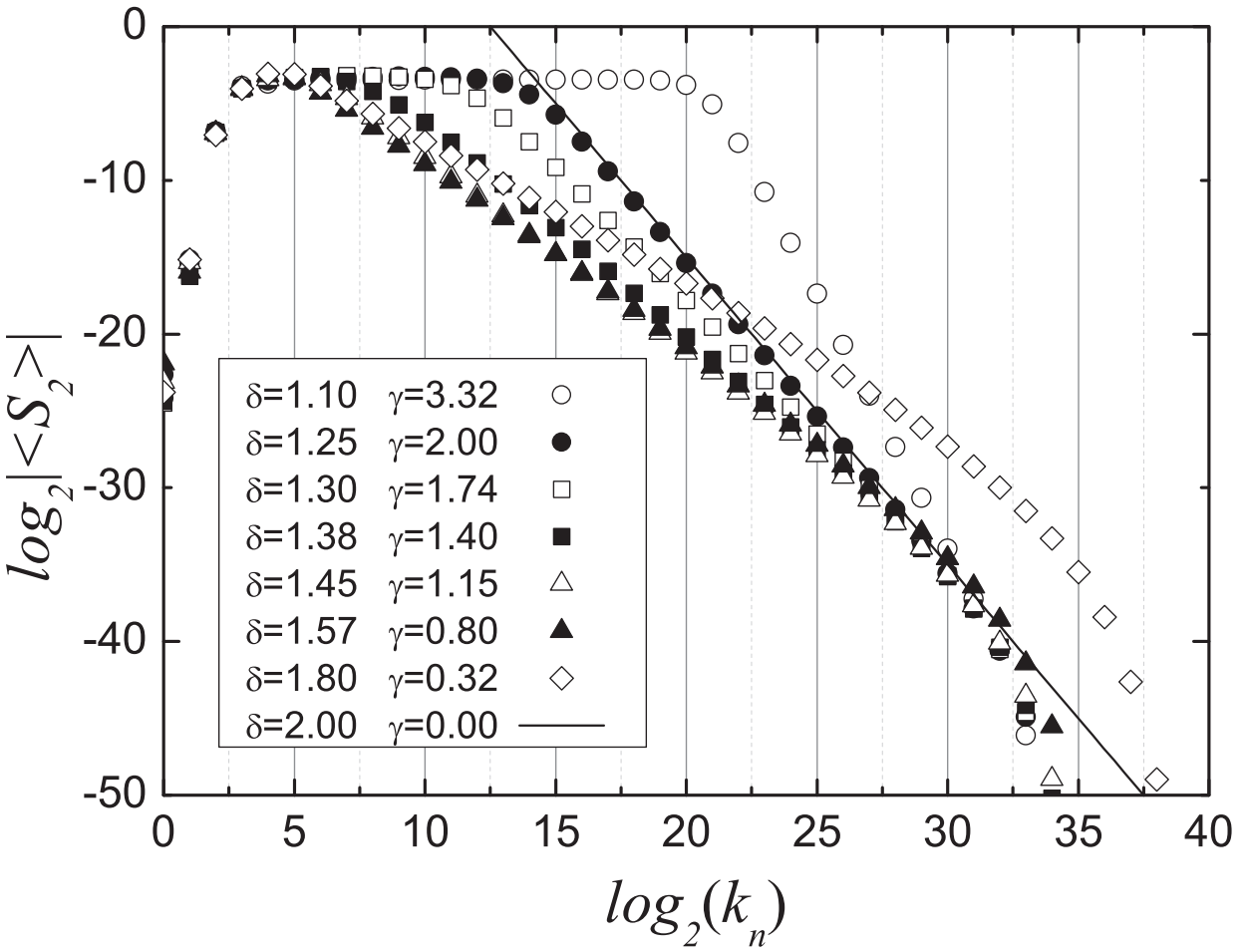

Fig. 3. A log-log plot of the second order structure functions of velocity as a function of k_n for different values of δ and γ.

$\gamma = 0.8$, buoyancy starts to reduce R more and more until a similar behavior of $R \sim k_n^{-1}$ and $R \sim k_n^{-1+3\gamma/2}$ is respectively setup as the Sabra model in the scaling range of $k_n < k_c$ and $k_n > k_c$ for $1 < \delta < 1.25$. Thus, buoyancy may influence the scaling behavior of the SabraT model and BO scaling is possibly available only in the range of $1.25 \le \delta \le 1 + 2^{-0.8}$ or $0.8 \le \gamma \le 2$.

As seen from Fig. 2, the skewness $R(k_n)$ and the cross correlation function $R_c(k_n)$ measured in the SabraT model are shown together with varying δ, which clearly shows that R and R_c are almost scale independent with $\rho = \rho_c = 0$ only in the case of $\delta = 1 + 2^{-0.8}$ and $\gamma = 0.8$. R_c is larger and smaller than R for δ below and above $1 + 2^{-0.8}$, respectively. As discussed above, $\rho = \rho_c$ is required for the existence of BO scaling, which suggests that BO scaling is only observed at a critical parameter, $\delta = 1 + 2^{-0.8}$, rather than in a range, i.e., the parameter independent BO scaling is unavailable for the SabraT model. By comparing the R and R_c values in Fig. 2, one can easily reveal the reason why BO scaling is unavailable in the SabraT model.

Moreover, as seen from Fig. 2(a), numerical value of R_c is much smaller than 0.03 in the range of $1 < \delta < 1.25$, which indicates why buoyancy is irrelevant in this range. As seen from Fig. 2(b), numerical value of R_c is not much smaller than 0.03 in the range of $1.25 \le \delta \le 1 + 2^{-0.8}$, indicating that buoyancy is relevant in this range with a new modified scaling behavior deviates from the Sabra model.

As seen from Fig. 3, the scaling behavior of velocity for the SabraT model is dependent on parameter δ or γ. Numerical results show that the scaling exponent of the second order velocity structure function, ζ_2, decreases as δ increasing. Moreover, for $1 < \delta < 1 + 2^{-1.4}$ (See also $\gamma > 1.4$), i.e., $1 < \delta < 1.38$, there exists dual scaling ranges; while for $1 + 2^{-1.4} < \delta < 2$ or $0 < \gamma < 1.4$, only one scaling range exists. As seen from Figs. 4–6, detailed description of the different scaling behaviors of $S_2 \sim k_n^{-\zeta_2}$ are shown by a compensated form of $S_2 k_n^{\eta} \sim k_n^{\eta-\zeta_2}$ with different compensated exponents η. Clearly, when the compensated structure function is scale independent with constant value, one gets the different γ dependent scaling exponents of $\zeta_2 = \eta$ that are shown in Fig. 7.

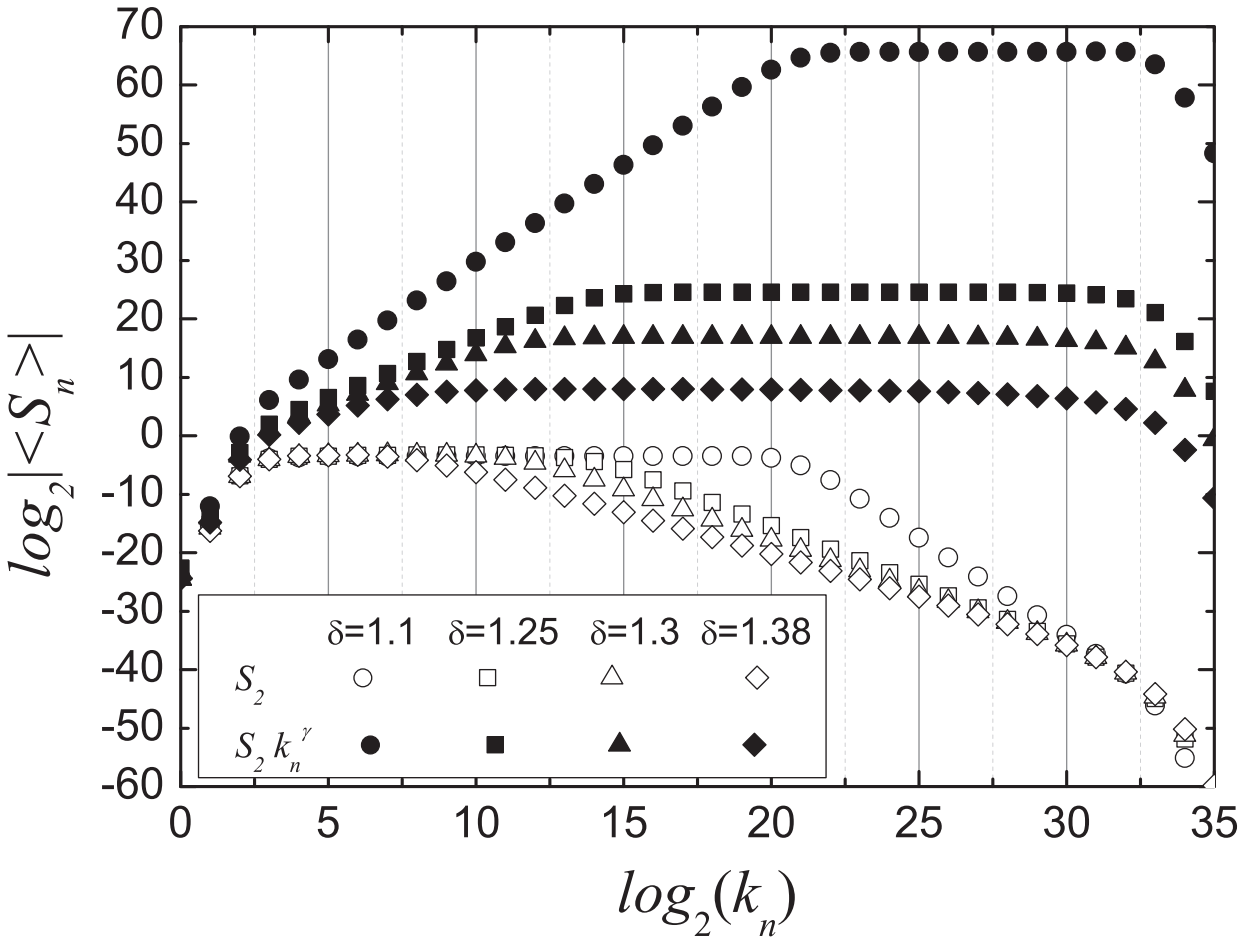

Fig. 4. A log-log plot of $\langle S_2 \rangle$ (open symbols) and $\langle S_2 k_n^{\gamma} \rangle$ (closed symbols) as a function of k_n for different values of δ in the range of $1 < \delta \leq (1 + 2^{-1.4} \approx 1.38)$. Closed symbols denote the energy equipartition scaling, and open symbols denote the enstrophy equipartition scaling.

Apart from $\delta = 1.25$ (See also $\gamma = 2$), there are another two critical parameters, i.e., $\delta = 1 + 2^{-1.4}$ (See also $\gamma = 1.4$) and $\delta = 1 + 2^{-0.8}$ (See also $\gamma = 0.8$). These three critical parameters separate the range of $1 < \delta < 2$ or $\gamma > 0$ into four regimes that denote as regime(I), (II), (III) and (IV), i.e., $1 < \delta < 1.25$ or $\gamma > 2$ for regime (I), $1.25 < \delta < 1 + 2^{-1.4}$ or $1.4 < \gamma < 2$ for regime (II), $1 + 2^{-1.4} < \delta < 1 + 2^{-0.8}$ or $0.8 < \gamma < 1.4$ for regime (III) and $1 + 2^{-0.8} < \delta < 2$ or $0 < \gamma < 0.8$ for regime (IV).

In regime (I) and (II), energy and enstrophy equipartition scaling are respectively observed with $\zeta_2 = 0$ and $\zeta_2 = \gamma$ in the range of $k_n < k_c$ and $k_n > k_c$, which is shown in Fig. 4. Moreover, k_c increases with decreasing δ, which is discussed in the following section.

In regime (II), enstrophy cascade scaling is observed in the range of $k_n > k_c$ for the Sabra model. However, enstrophy equipartition scaling $\zeta_2^{II} = \gamma$ is observed in regime (II) for the SabraT model, which suggests that buoyancy changes the scaling behavior of the SabraT model in this regime.

As shown in Fig. 5, in regime (IV), enstrophy cascade scaling is observed with $\zeta_2^{IV} = 2(1 + \gamma)/3$. The above scaling features in regime (I) and (IV) are similar to the original Sabra model, which suggests that buoyancy is irrelevant in these regimes as discussed above.

Fig. 6 displays the scaling behaviors with different scaling exponents of η in regime (III). It is clearly demonstrated that neither the enstrophy cascade and equipartition scaling with $\zeta_2 = 2(1 + \gamma)/3$ and $\zeta_2 = \gamma$ nor the BO scaling with $\zeta_2 = 6/5$ is available in this buoyant relevant range. However, a new interpolated scaling exponent with $\zeta_2^{III} = \frac{2(1+\gamma)/3+6/5}{2} = \frac{5\gamma+14}{15}$ is setup in this regime, i.e., the scaling exponent is equal to the average of the enstrophy cascade scaling exponent and BO scaling exponent. Thus, when buoyancy is relevant in regime (III), the scaling behavior equivalently deviates both from the BO scaling and enstrophy cascade scaling.

Conclusively, the scaling behavior relates to the enstrophy equipartition scaling in regime (I) and (II); whereas, it relates to the enstrophy cascade scaling in regime (III) and (IV). Thus, the velocity scaling behavior is mainly determined by the budget equation of enstrophy, instead of the budget equation of energy. As $\gamma > 0$ in the range of $1 < \delta < 2$, the containing enstrophy at each shell is getting more than the containing energy at each shell with increasing k_n and γ. No surprise, then,

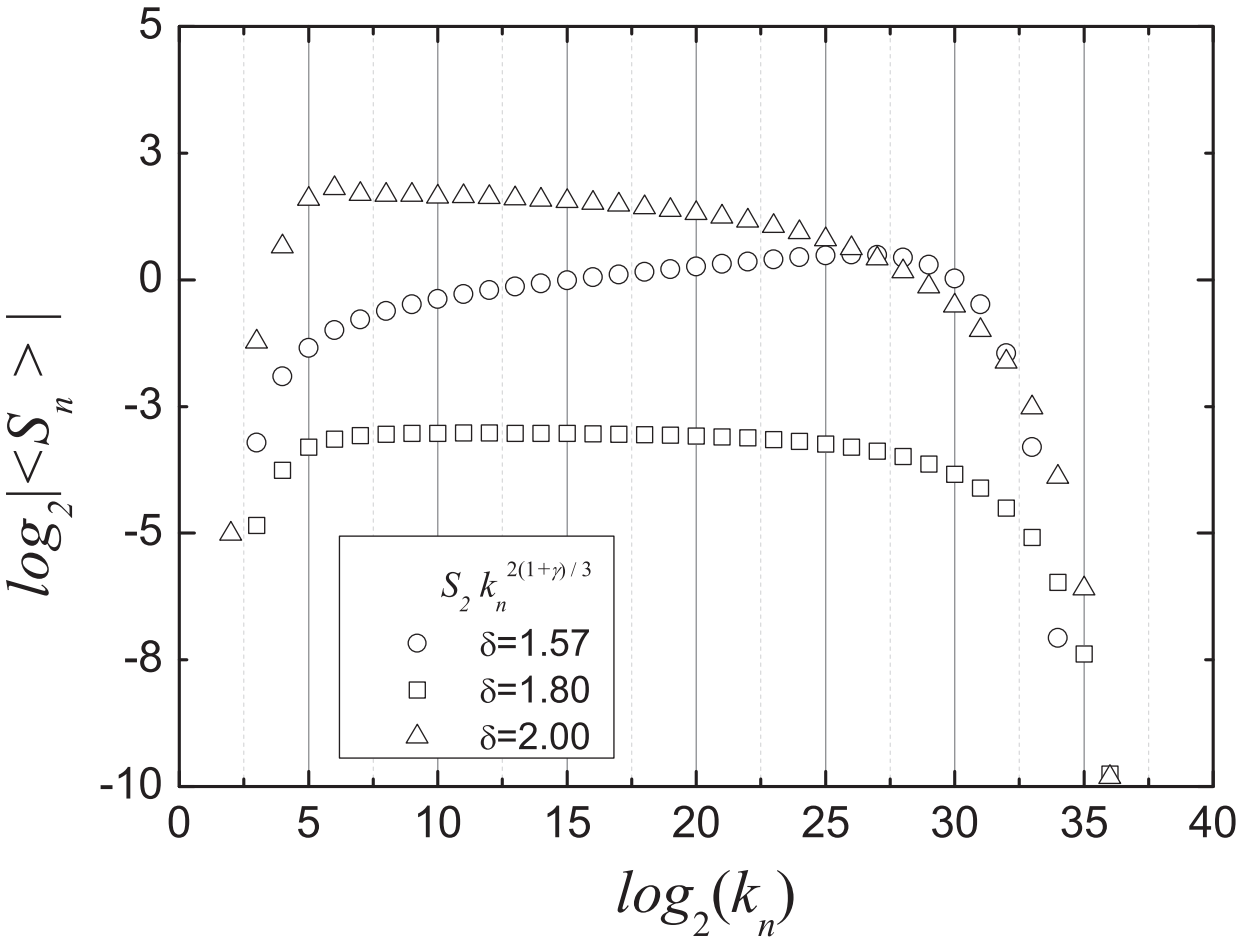

Fig. 5. A log-log plot of $\left\langle S_2 k_n^{2(1+\gamma)/3} \right\rangle$ as a function of k_n for different δ in the range of $(1+2^{-0.8} \approx 1.57) \le \delta \le 2$.

it is the enstrophy budget equation plays a leading role in the SabraT model for $1 < \delta < 2$, instead of the energy budget equation.

4. Buoyancy effects of the SabraT model

To theoretically give the critical parameters that separates the four regimes, we focus on studying the buoyancy effects on the scaling behavior of the SabraT model in the range of $1+2^{-1.4} \le \delta \le 2$, i.e., regime (III) and (IV), where the scaling behavior is found to be influenced and uninfluenced by buoyancy, respectively.

As shown in the inset of Fig. 8, the rate of entropy flux, F_θ, is independent of k_n in the scaling range with varying δ, indicating that the entropy cascade is always set up for the SabraT model. As shown in Fig. 8, the validity of dimensional analysis of Eq. (32) is checked by a log-log plot of $\langle \varepsilon_\theta \rangle^{-1} k_n \langle S_2 \rangle^{1/2} \langle R_2 \rangle$ as a function of k_n for different δ. Clearly, dimensional analysis is correct in regime (III) and (IV) for $1+2^{-1.4} \le \delta \le 2$, which gives the relation between ζ_2 and ξ_2 as Eq. (32). However, dimensional analysis is incorrect in regime (I) and (II) for $1 < \delta < 1+2^{-1.4}$ when enstrophy equipartition scaling is set up. Thus, the first condition of Eq. (33) is satisfied in regime (III) and (IV).

As shown in Fig. 9, the different terms in the energy and enstrophy budget equations, Eq. (5) and (6), are shown together with the total local energy and enstrophy dissipation rates, i.e., ε_u and $\tilde{\varepsilon}_u$. In regime (IV), it is clearly shown in Fig. 9(a)–(c) that the injected enstrophy due to buoyancy is much smaller than the rate of enstrophy flux which equals to the total local enstrophy dissipation rate, i.e., $\langle \tilde{F}_u \rangle \approx \varepsilon_u \gg \langle \tilde{P}_u \rangle$. A forward enstrophy cascade is set up in the whole scaling range with irrelevant buoyancy that acts like an external force only applied on the largest scales. However, dual energy cascades with opposite transfer directions are setup in the whole scaling range. At $k_0 \ll k_n < k_{n^*}$, energy is transferred backward, which is not constant in wavenumber due to the effects of buoyancy. Whereas, at $k_{n^*} < k_n \ll k_d$, energy is transferred forward with constant value. This phenomenon may be due to the coexistence of 2D and 3D-like turbulence in the system. As discussed by Boffetta et al. [8] and Zhou et al. [9], for 2D convection turbulence, buoyancy is comparable to the inertial forcing, the kinetic energy is, on average, dynamically transferred to large scales by an inverse cascade, while both entropy and

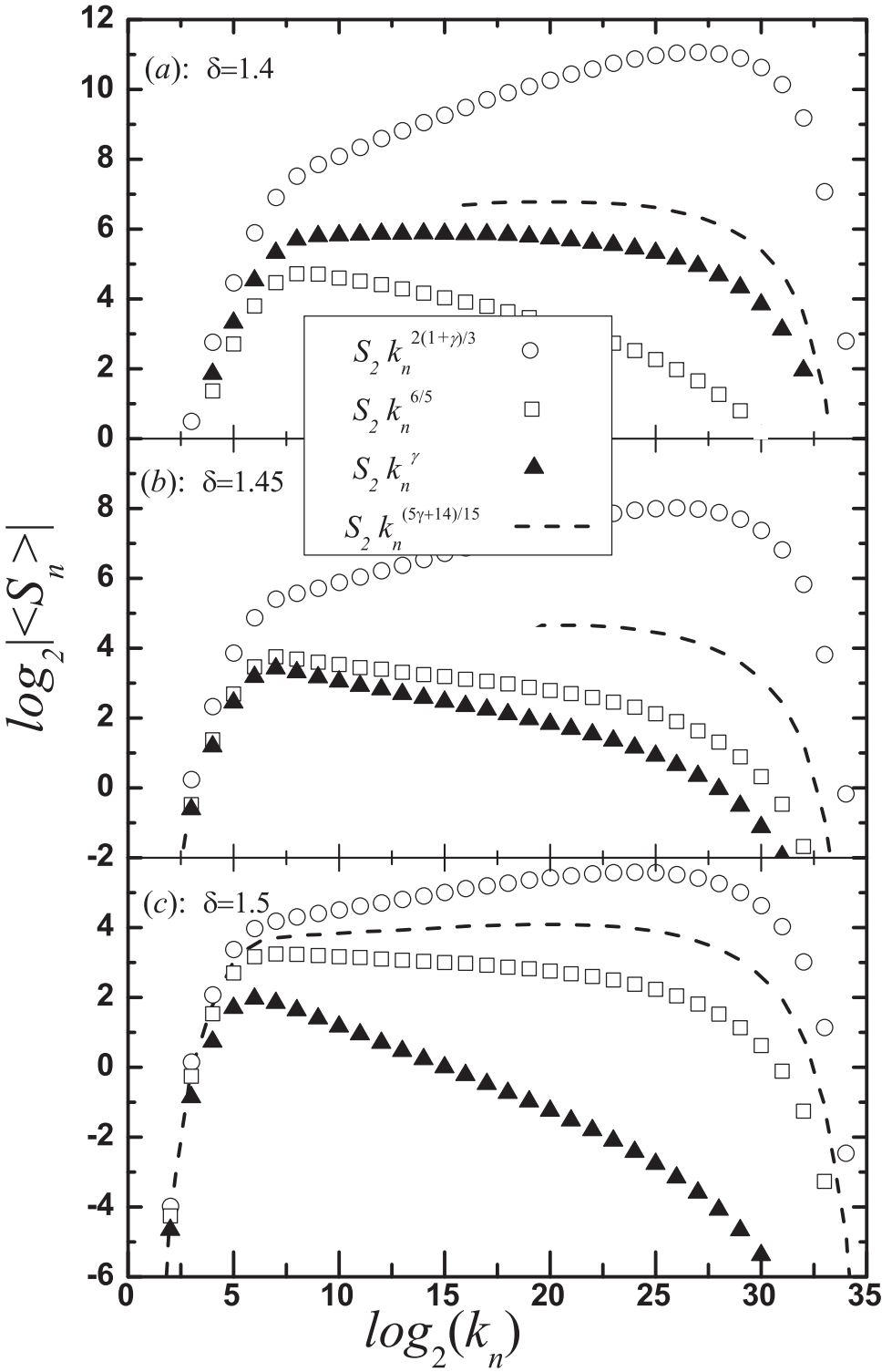

Fig. 6. A log-log plot of $\langle S_2 k_n^{\eta} \rangle$ as a function of k_n with different scaling exponents of η for different δ in the range of $(1+2^{-1.4} \approx 1.38) \leq \delta \leq (1+2^{-0.8} \approx 1.57)$. Here, $\eta = 2(1+\gamma)/3$ (circle) is the enstrophy cascade scaling exponent, $\eta = 6/5$ is the BO scaling exponent (squares), $\eta = \gamma$ is the enstrophy equipartition scaling exponent (triangles) and $\eta = (5\gamma + 14)/15$ is the new interpolated scaling exponent (dash line).

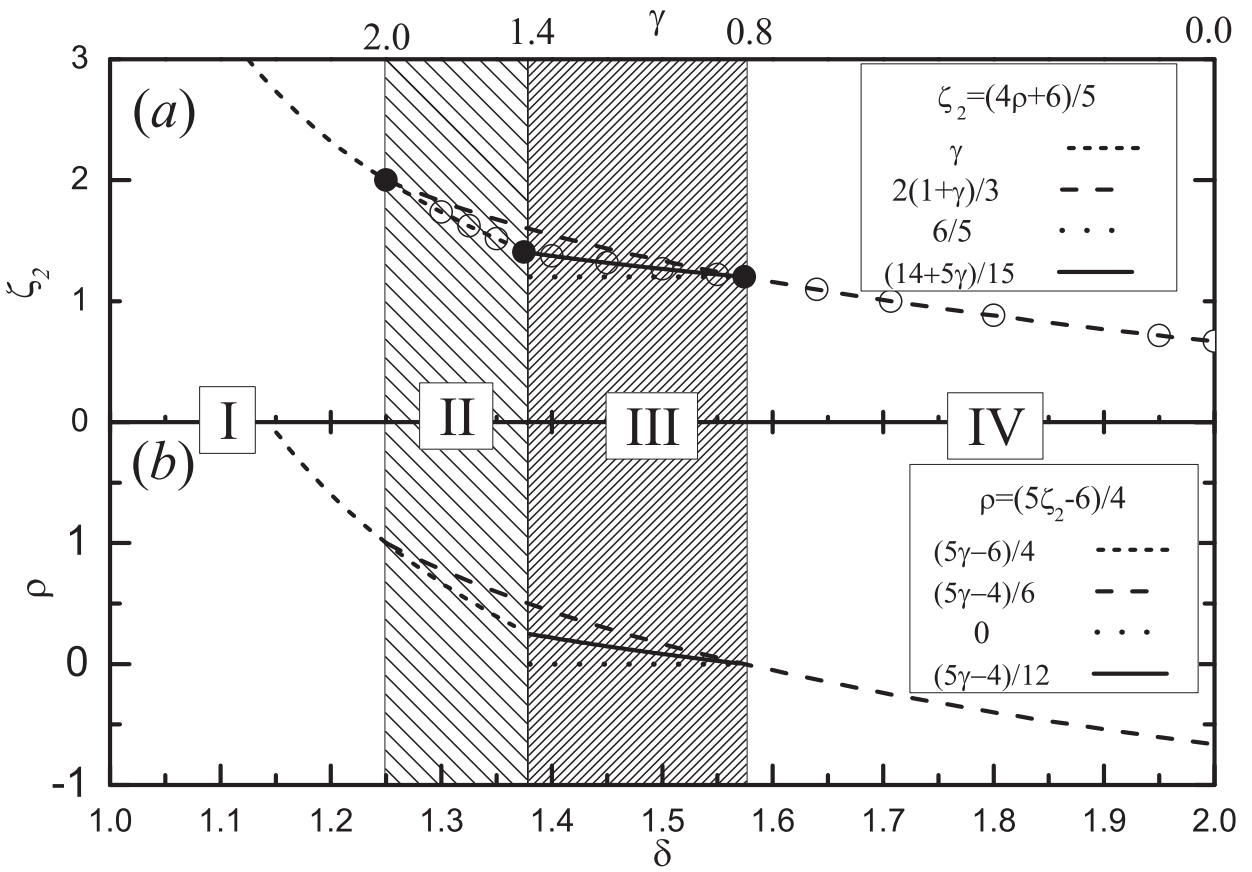

Fig. 7. The parameter dependent scaling exponents of, $(a)\zeta_2 = (4+\rho)/5$ and $(b)\rho = (5\zeta_2 - 6)/4$ as a function of δ measured in the Sabra model. The short-dash lines show the enstrophy equipartition scaling exponents of (a): $\zeta_2 = \gamma$ and (b): $\rho = (5\gamma - 6)/4$ that observed in regime (I and II). The dash lines show the enstrophy cascade scaling exponents of (a): $\zeta_2 = 2(1+\gamma)/3$ and (b): $\rho = (5\gamma - 4)/6$ that observed in regime (IV). The lines show the interpolated scaling exponents of (a): $\zeta_2 = (14+5\gamma)/15$ and (b):$\rho = (5\gamma - 4)/12$ that observed in regime (III). The lines show the BO scaling exponents of (a): $\zeta_2 = 6/5$ and (b): $\rho = 0$, which is only observed for $\delta \approx 1.57$ or $\gamma = 0.8$.

enstrophy move towards small scales by forward cascades. But for real 3D convective turbulence, buoyancy is insignificant and is much smaller than inertial forcing, kinetic energy moves towards small scales by forward cascade. From the view point of energy and enstrophy cascades, the large-scale flow satisfies the 2D-like turbulent features while the small-scale flow satisfies the 3D-like turbulent features.

However, in regime (III), it is shown in Fig. 9(d)–(f) that the buoyancy term of P_n or $\tilde{P}_n$ is comparable to the transfer term of F_u or $\tilde{F}_u$ at $k_0 \ll k_n \ll k_d$, indicating that buoyancy terms play a role in both energy and enstrophy equations. Moreover, the critical scale k_{n^*} is not observed in this regime. Similar to the 2D-like turbulence, enstrophy and energy are transferred forward and backward in the whole scaling range, respectively.

The reason why dual energy transfer processes only appear at regime (IV) and k_{n^*} decreases with δ increasing are discussed as follows. As seen from Fig. 9, one gets $\varepsilon_u \sim \nu k_d^2 u_d^2$ and $\tilde{\varepsilon}_u \sim \nu k_d^{2+\gamma} u_d^2$, which gives $\tilde{\varepsilon}_u/\varepsilon_u \sim k_d^{\gamma}$. Thus, the difference between $\tilde{\varepsilon}_u$ and ε_u increases with increasing γ or deceasing δ, which is clearly shown in Fig. 9. However, the transfer flux of energy and enstrophy are of the same order at small scales close to k_0, which gives $F_u(k_0) \approx \tilde{F}_u(k_n) \approx \tilde{\varepsilon}_u$. When $\tilde{\varepsilon}_u \gg \varepsilon_u$, one gets $F_u(k_n) \ll F_u(k_0)$ in the scaling range, which suggests that $F_u(k_n) \sim F_u(k_0) \sim \varepsilon_u$ with a direct energy cascade is unset up in the whole scaling range, i.e., $F_u(k_n)$ decreases from a larger value of $F_u(k_0) \approx \tilde{\varepsilon}_u$ to a smaller value of ε_u. Thus, k_{n^*} increases with decreasing δ or increasing γ, and k_{n^*} is very close to k_d for $\delta = 1 + 2^{-0.8}$, as shown in Fig. 9(c). It can be excepted that $k_{n^*} > k_d$ when δ is further decreased, such that only the 2D-like feature can be observed in the whole scaling range in regime (III).

The critical shell k_{n^*} has been reported to be the buoyancy scale in the SabraT model in the range of $0 < \delta < 1$, above which buoyancy is relevant and significant in the energy budget equation [22]. However, in regime (IV), different effects of buoyancy in the energy and enstrophy budget equations are shown in the range of $k_0 \ll k_n < k_{n^*}$. As discussed above, it is the enstrophy budget equation that plays a leading role in the SabraT model. According to the behavior of the enstrophy budget equation, buoyancy is irrelevant and insignificant with a similar enstrophy cascade scaling behavior as the Sabra model that observed in the whole scaling range in regime (IV), even in the range of $k_0 \ll k_n < k_{n^*}$.

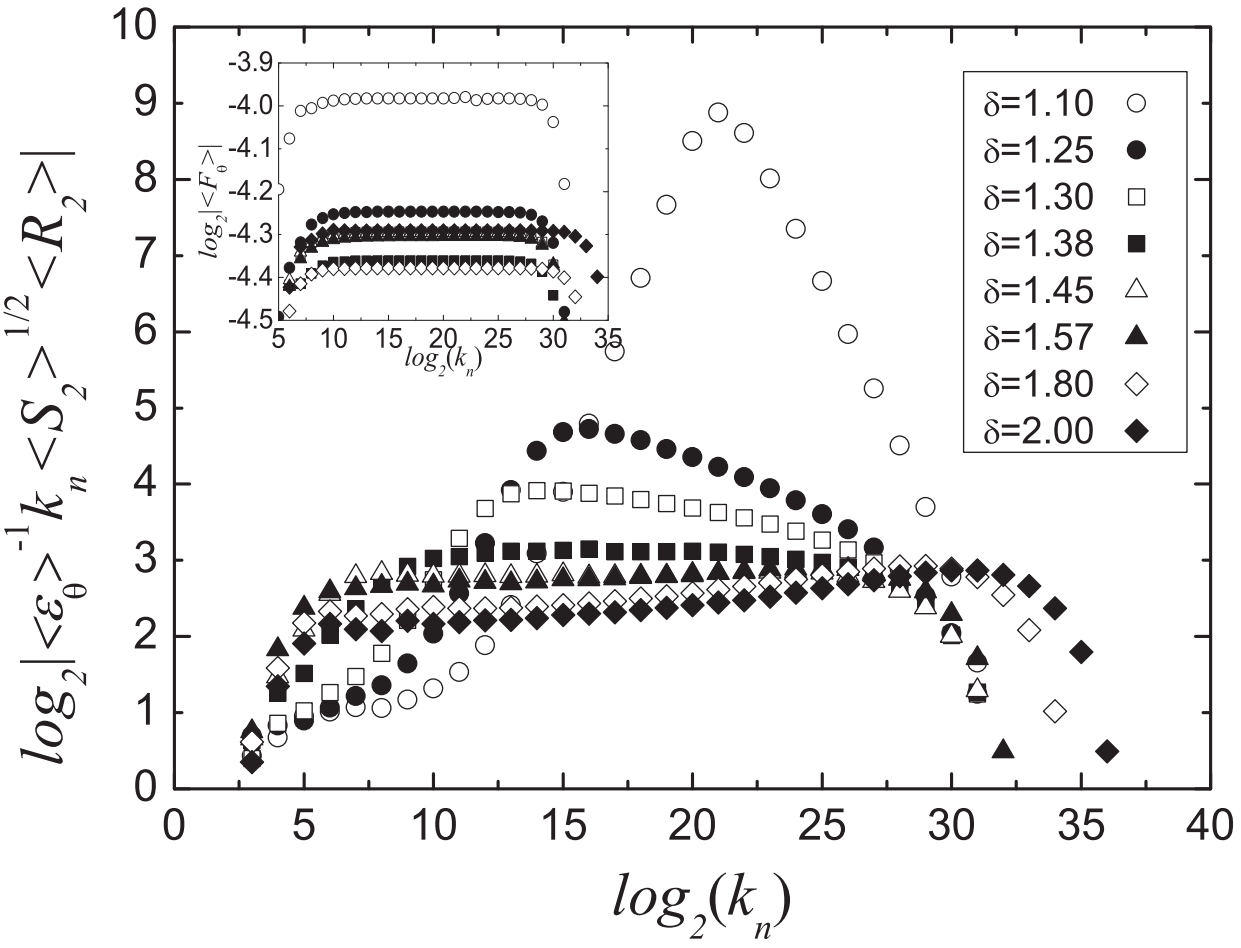

Fig. 8. A log-log plot of $\langle\varepsilon_\theta\rangle^{-1}k_n\langle S_2\rangle^{1/2}\langle R_2\rangle$ as a function of k_n for different δ in the range of $1 \le \delta \le 2$. Inset shows a log-log plot of $\langle F_\theta\rangle$ as a function of k_n.

Moreover, the difference between the transfer flux of enstrophy and injected enstrophy due to buoyancy decreases with decreasing δ, which suggests that buoyancy may start to be relevant at the critical parameter $\gamma = 0.8$ or $\delta = 1 + 2^{-0.8}$. As shown in Fig. 9(c), buoyancy is still irrelevant with $\tilde{F}_u \gg \tilde{P}_u$ for $\delta = 1 + 2^{-0.8}$. Thus, the above observed scaling exponent of 6/5 at $\gamma = 0.8$ is just a parameter dependent scaling behavior of $\zeta_2^{IV} = 2(1+\gamma)/3$, which suggests that BO scaling with relevant buoyancy effects is not setup in regime (IV).

In regime (III), it clearly shows in Fig. 9(d)–(f) that the injected enstrophy due to buoyancy stars to be relevant with the same scaling exponent as the transfer flux of enstrophy, i.e., $\rho_B = 0$. Thus, the scaling exponent of ζ_2 is expected to deviate from ζ_2^{IV}. According to Eq. (36), one gets $\zeta_2^{III} = (4\rho^{III} + 6)/5$ with $\rho_c^{III} = 0$ that plotted in Fig. 2(b). If $\zeta_2^{III} = \zeta_2^{IV}$, one gets $\rho_H = (5\gamma - 4)/6$, which suggests that ρ^{III} deviates from ρ_H due to buoyancy effects. According to Eq. (27), $\rho \ge \rho_L = 0$ is required and one gets $\rho_L \le \rho^{III} \le \rho_H$. As shown in Fig. 7(b), numerical results show that ρ^{III} just stays in the middle of the two cures with $\rho^{III} = (\rho_L + \rho_H)/2 = (5\gamma - 4)/12$ in regime(III), which gives the corresponding $\zeta_2^{III} = (14 + 5\gamma)/15$. As $\zeta_2^{II} = \gamma$ is observed in regime (II), which suggests that $\gamma = 1.4$ or $\delta = 1 + 2^{-1.4} \approx 1.38$ is the borderline between regime (II) and (III) with the same value of $\zeta_2^{II} = \zeta_2^{III} = 1.4$.

5. Conclusions

Both Brandenburg and SabraT model have been proposed for turbulent thermal convection. However, it has been reported that the Bolgiano-Obukhov scaling behavior is only observed in the Brandenburg model with suitable parameters. For the SabraT model, it has been reported that K41 scaling is observed in the range of $0 < \delta < 1$. In this paper, we explains why Bolgiano-Obukhov scaling behavior is unavailable in the SabraT model for $1 < \delta < 2$, i.e., $\gamma = -log_2(\delta - 1) > 0$. As k_n^γ measures the ratio of enstrophy to energy with $\gamma > 0$, the containing enstrophy at each shell is getting more than the containing energy at each shell with increasing k_n and γ. No surprise, then, it is the enstrophy budget equation plays a leading role in the SabraT model for $1 < \delta < 2$, instead of the energy budget equation. From numerical results, we find

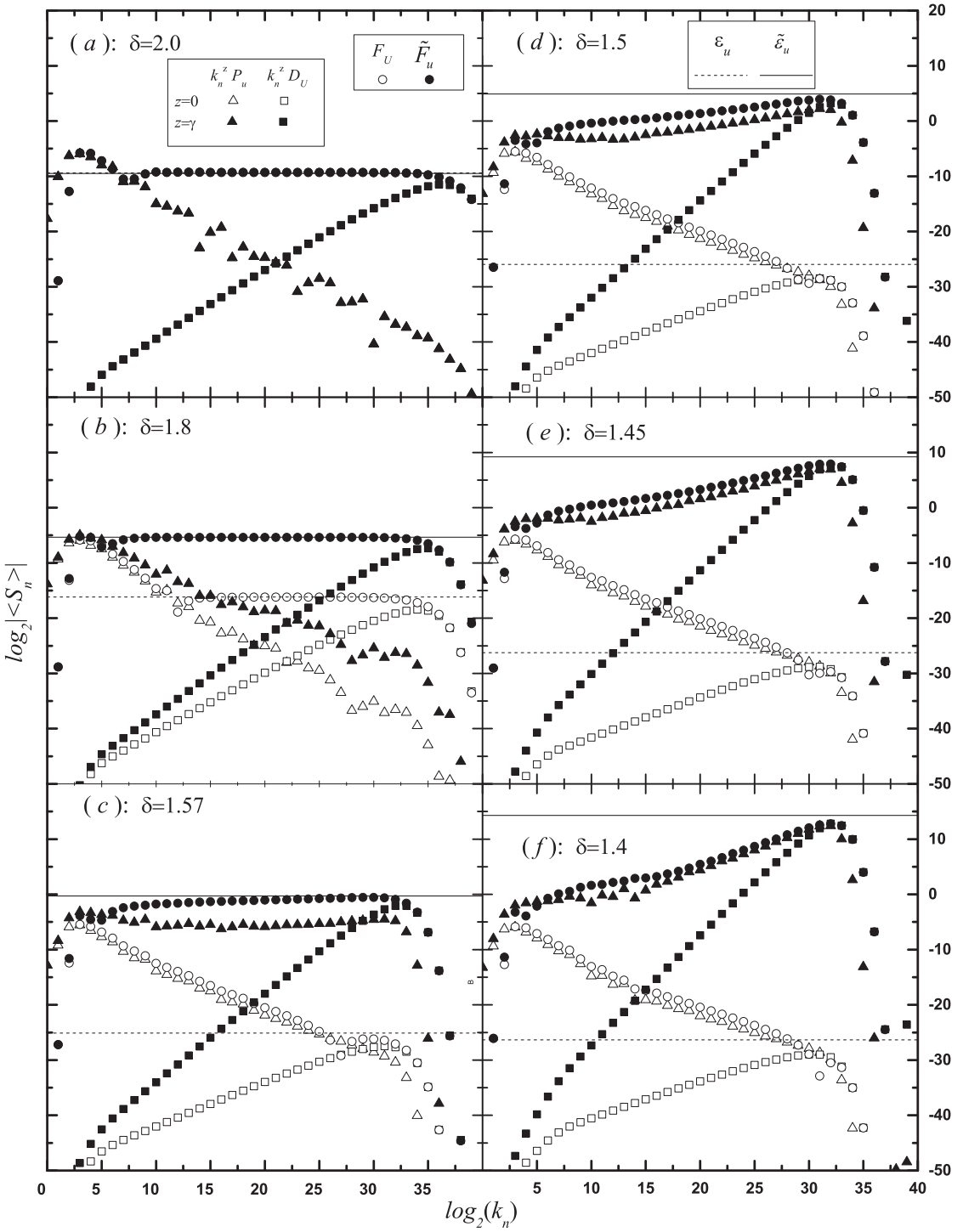

Fig. 9. A log-log plot of the different terms in Eq. (5) (open symbols) and (6) (closed symbols) as a function of k_n for $1.58 \leq \delta \leq 2$(regime IV). Here, F_u (open circles) and $\tilde{F}_u$ (closed circles) are respectively the transfer flux of energy and enstrophy in each shell. D_u (open squares) and $\tilde{D}_u$ (closed squares) are respectively the dissipation of energy and enstrophy in each shell. P_u (open triangles) and $\tilde{P}_u$ (closed triangles) are respectively the injected energy and enstrophy due to buoyancy in each shell. ε_u (dash line) and $\tilde{\varepsilon}_u$ (solid line) are respectively the total local dissipation of energy and enstrophy rates in each shell.

that the scaling behavior of velocity is dependent on the parameter γ with different buoyancy effects observed at four regimes, i.e., regime (I), (II), (III) and (IV). Comparatively, the different scaling behaviors are investigated by observing the variation of two dimensionless parameters R and R_c in these regimes. R_c is the cross correlation function of velocity and temperature that measures the effects of buoyancy. R is the skewness that measures the deviation of the enstrophy flux rate from dimensional analysis, which plays an import role in the scaling behavior of velocity. In regime (I) and (IV), R is of the same behavior as the Sabra model, which suggests that a similar γ-dependent scaling behavior is setup for the SabraT model, i.e., an energy/enstrophy equipartition scaling is observed in regime (I) and an enstrophy cascade scaling is observed in regime (IV). In regime (II) and (III), R is reduced by the existence of buoyancy that clearly indicated by the observed larger values of R_c, which suggests that different scaling behaviors are observed for the Sabra and SabraT model in these regimes. In regime (II), R is reduced to a similar behavior that observed in regime (I), which suggests that an enstrophy equipartition scaling is also observed in regime (II). In regime (III), R_c is found to be larger than R and a direct transport of enstrophy is still observed with smaller parameter R, which suggests that the introduced buoyancy plays as a relative small perturbed forcing on the Sabra model without changing its intrinsical statistical properties, i.e., a new γ-dependent scaling behavior that equivalently deviates from the enstrophy cascades scaling and BO scaling is setup in this regime, instead of the parameter γ-independent BO scaling.

Acknowledgments

This work was supported by the National Natural Science Foundation of China (Grant No. 11272034) and the China-EU Aeronautical Science & Technology Cooperation Project DRAGY.

References

[1] Siggia ED. High rayleigh number convection. Ann Rev Fluid Mech 1994;26:137–68.
[2] Ahlers G, Grossmann S, Lohse D. Heat transfer and large scale dynamics in turbulent rayleighCB 'enard convection. Rev Mod Phys 2009;81(2):503C537.
[3] Lohse D, Xia KQ. Small-scale properties of turbulent rayleigh-benard convection. Annu Rev Fluid Mech 2010;42:335–64.
[4] L'vov VS. Spectra of velocity and temperature fluctuations with constant entropy flux of fully developed free-convective turbulence. Phys Rev Lett 1991;67:687–90.
[5] Bolgiano R. Turbulent spectra in a stably stratified atmosphere. J Geophys Res 1959;64:2226–9; Obukhov AM. Effect of archimedean forces on the structure of the temperature field in a turbulent flow. Dokl Akad Nauk SSSR 1959;125:1246–8.
[6] Ching E.S.C., Cheng W.C.. Anomalous scaling and refined similarity of an active scalar in a shell model of homogeneous turbulent convection. Phys Rev E 2008 77. 015303(R)-015306(R).
[7] Ching ESC, Guo H, Lo TS. Refined similarity hypotheses in shell models of homogeneous turbulence and turbulent convection. Phys Rev E 2008a;78:026303–13.
[8] Boffetta G, De Lillo F, Mazzino A, Musacchio S. Bolgiano scale in confined rayleigh-taylor turbulence. J Fluid Mech 2011a;690:426–40.
[9] Zhou Q, Huang YX, Lu ZM, Liu YL, Ni R. Scale-to-scale energy and enstrophy transport in two-dimensional rayleigh-taylor turbulence. Journal of Fluid Mechanics 2015;786:294–308.
[10] Kolmogorov AN. The local structure of turbulence in incompressible viscous fluid for very large reynolds numbers. C R Acad Sci URSS 1941;30:301–5.
[11] Ching ESC, Chui KW. Velocity and temperature cross-scaling in turbulent thermal convection. J Turb 2004;5(1):027–37.
[12] Zhou Q, Xia KQ. Comparative experimental study of local mixing of active and passive scalars in turbulent thermal convection. Phys Rev E 2008;77:056312–23.
[13] Biferale L. Shell models of energy cascade in turbulence. Ann Rev Fluid Mech 2003;35:441–68.
[14] Bohr T, Jensen MH, Paladin G. Dynamical systems approach to turbulence. Cambridge: Cambridge University Press; 1998.
[15] Guo H, Li C, Qu QL, Liu PQ. Attractive fixed-point solution study of shell model for homogeneous isotropic turbulence. J Appl Math Mech 2013a;34(3):259–68.
[16] Gledzer EB. Hydrodynamic-type system admitting two quadratic integrals of motion. Dokl Akad Nauk SSSR 1973;209:1046–8; Ohkitani K, Yamada M. Temporal intermittence in the energy cascade process and local lyapunov analysis in fully developed turbulence. Prog Theor Phys 1989;89:329–41.
[17] L'vov VS, Podivilov E, Pomyalov A. Improved shell model of turbulence. Phys Rev E 1998;58:1811–22.
[18] Ditlevsen PD, Mogensen IA. Cascades and statistical equilibrium in shell models of turbulence. Phys Rev E 1996;53(5):4785–93.
[19] Thomas G, Victor SL, Anna P, Itamar P. Inverse cascade regime in shell models of two-dimensional turbulence. Phys Rev Lett 2002;89:074501.
[20] Brandenburg A. Energy spectra in a model for convective turbulence. Phys Rev Lett 1992;69:605–8.
[21] Suzuki E, Toh S. Entropy cascade and temporal intermittency in a shell model for convective turbulence. Phys Rev E 1995;51:5628–35.
[22] Ching ESC, Guo H, Cheng WC. Understanding the different scaling behavior in various shell models proposed for turbulent thermal convection. Physica D 2008b;237:2009–14.
[23] Guo H, Li C, Qu QL, Liu PQ. Attractive fixed-point solution study of a shell model for turbulent convection. J Sci Chin Phys Mech Astron 2013b;56(5):995–1003.
[24] Jiang MS, Liu SD. Scaling behavior of velocity and temperature in a shell model for thermal convective turbulence. Phys Rev E 1997;56:441–6.
[25] Guo H. Statistics and structures in turbulent thermal convection. The Chinese University of Hong Kong; 2007. Ph.d. thesis.
[26] Boffetta G, De Lillo F, Musacchio S. Shell model for quasi-two-dimensional turbulence. Phys Rev E 2011b;83:066302–7. 2011
[27] Khani S, Waite ML. Buoyancy scale effects in large-eddy simulations of stratified turbulence. J Fluid Mech 2014a;754:75–97.
[28] Khani S, Waite ML. Effective eddy viscosity in stratified turbulence. J of Turbl 2014b;14(7):49–70.
[29] Waite ML, Bartello P. Stratified turbulence dominated by vortical motion. J Fluid Mech 2004;517:281–308.
[30] Khani S, Waite ML. Large eddy simulations of stratified turbulence: the dynamic smagorinsky model. J Fluid Mech 2015;773:327–44.
[31] Lindborg E. The energy cascade in a strongly stratified fluid. J Fluid Mech 2006;550:207.
[32] Riley JJ, de Bruyn KSM. Dynamics of turbulence strongly influenced by buoyancy. Phys Fluids 2003;15:2047.
[33] Kumar A, Verma MK. Shell model for buoyancy-driven turbulence. Phys Rev E 2015;91:043014–19.